# Microstructure and interface studies of $LaVO_3/SrVO_3$ superlattices

P. Boullay,[1] A. David,[1] W. C. Sheets,[1] U. Lüders,[1] W. Prellier,[1] H. Tan,[2] J. Verbeeck,[2] G. Van Tendeloo,[2] C. Gatel,[3] G. Vincze,[4] and Z. Radi[4]

[1]*CRISMAT, ENSICAEN, CNRS UMR 6508, 6 Boulevard Maréchal Juin, F-14050 Caen Cedex 4, France*

[2]*EMAT, University of Antwerp, Groenenborgerlaan 171, B-2020 Antwerpen, Belgium*

[3]*CEMES, CNRS UPR 8011, 29 rue Jeanne Marvig, F-31055 Toulouse Cedex 4, France*

[4]*Technoorg Linda Scientific Technical Development Ltd., Rozsa utca 24, H-1077 Budapest, Hungary*

(Received 4 November 2010; published 9 March 2011)

The structure and interface characteristics of $(LaVO_3)_{6m}(SrVO_3)_m$ superlattices deposited on a (100)-$SrTiO_3$ substrate were studied using transmission electron microscopy (TEM). Cross-section TEM studies revealed that both $LaVO_3$ (LVO) and $SrVO_3$ (SVO) layers are good single-crystal quality and epitaxially grown with respect to the substrate. It is evidenced that LVO layers are made of two orientational variants of a distorted perovskite compatible with bulk $LaVO_3$, while SVO layers suffers from a tetragonal distortion due to the substrate-induced stain. Electron energy loss spectroscopy investigations indicate changes in the fine structure of the V $L_{23}$ edge, related to a valence change between the $LaVO_3$ and the $SrVO_3$ layers.

DOI: 10.1103/PhysRevB.83.125403 PACS number(s): 68.37.−d, 68.65.Cd, 73.21.Cd

## I. INTRODUCTION

Oxide superlattices constitute a group of materials where an artificial periodicity of ultrathin films made of two different oxides is created. The properties of superlattices are governed by the interplay of a number of effects such as reduced dimensions and distortion of the lattice due to the mismatch between the constituents and the orbital physics. In such systems, the physical properties of interfaces can be quite surprising, as seen for the complex behavior of polar discontinuous interfaces, showing a high-mobility two-dimensional (2D) electron gas,[1–5] magnetic effects at the interface of nonmagnetic materials,[6] or even superconductivity.[7] Most of these effects were observed at the $SrTiO_3/LaAlO_3$ interface. Another large group of systems showing a polar discontinuous interface, that is, $LaBO_3/SrBO_3$ (001)-oriented interfaces, with B being a transition metal, has received much less interest, although the phase diagrams of the solid solutions can indeed be very complex, showing interesting effects such as colossal magnetoresistance and charge ordering,[8] metal-to-insulator transitions,[9] and complete spin polarization of the conducting electrons.[10]

Recently, we have concentrated on $LaVO_3/SrVO_3$ superlattices since the properties of the parent compounds and of the solid solution show peculiar transitions, which would allow distinction between an interface and a 3D effect. For example, $LaVO_3$ is a Mott insulator, showing an antiferromagnetic transition at 143 K and a structural transition at 141 K.[11] $SrVO_3$, in contrast, is a cubic perovskite, nonmagnetic and metallic over the entire measured temperature range.[12] The solid solution $La_{1-x}Sr_xVO_3$ shows a metal-to-insulator transition at $x \approx 0.2$.[13–15] A series of epitaxial $(LaVO_3)_{6m}(SrVO_3)_m$ superlattices having the same nominal composition as $La_{6/7}Sr_{1/7}VO_3$, a Mott-Hubbard insulator, was grown,[16,17] and their superlattice period varied [see Fig. 1(a) as an illustration]. When $m = 1$, the transport properties vary from those of a bulk-like $La_{6/7}Sr_{1/7}VO_3$ insulator[16,17] to those of an interesting metallic phase,[18] depending on the deposition parameters. An increase in the periodicity of the superlattice (i.e., increase in the $m$ value) results in metallic samples.[16,17] In this paper, using transmission electron microscopy (TEM), we report microstructural and interface studies of some $(LaVO_3)_{6m}(SrVO_3)_m$ superlattices having the same properties as those reported in the papers by Sheets *et al.*[16,17]

## II. EXPERIMENTAL PROCEDURE

Samples were prepared by pulsed laser seposition on (100)-$SrTiO_3$ substrates; details are described elsewhere.[16] X-ray diffraction showed a cube-on-cube epitaxy of the superlattices, with a slightly tetragonally distorted perovskite structure ($a_c/c = 0.388$ nm/0.395 nm $= 0.98$, where $a_c$ is the in-plane lattice parameter of the pseudocubic representation and $c$ is the out-of-plane lattice parameter). A large number of orders of superlattice satellites at the main Bragg peaks indicates a high structural quality.[17] Selected samples were sectioned with a diamond-powder-coated sawing wheel, encapsulated in a titanium frame (3-mm disk), and thinned to 50 $\mu$m with SiC abrasive paper and fine-grain diamond paste. The mechanical preprocessing was followed by chemical cleaning and low-angle, high-energy ion milling (IV4/H/L; Technoorg Ltd.). The electron transparent samples were achieved with a dedicated low-energy ion mill (7°; 1000 and 250 eV) from the Technoorg Gentle Mill series. Selected-rea electron diffraction (SAED) and high-resolution electron microscopy (HREM) images were obtained using a JEOL 2010F microscope from these cross-section specimens. High-angle annular dark-field (HAADF) imaging and electron energy loss spectroscopy (EELS) were performed on a JEOL 3000F microscope. The EELS spectrometer was a Gatan GIF2000 1 K phosphor system used at an energy dispersion of 0.5 eV/channel and an approximate energy resolution of 1 eV. EELS scans in STEM mode were performed across the layer interfaces with a collection angle of 28.6 mrad and a convergence angle of 10.4 mrad. Geometric phase analysis (GPA)[19,20] was performed using the DigitalMicrograph GPA plug-in on HREM images obtained with a Tecnai F20 microscope equipped with a Cs corrector to avoid delocalization effects.

 

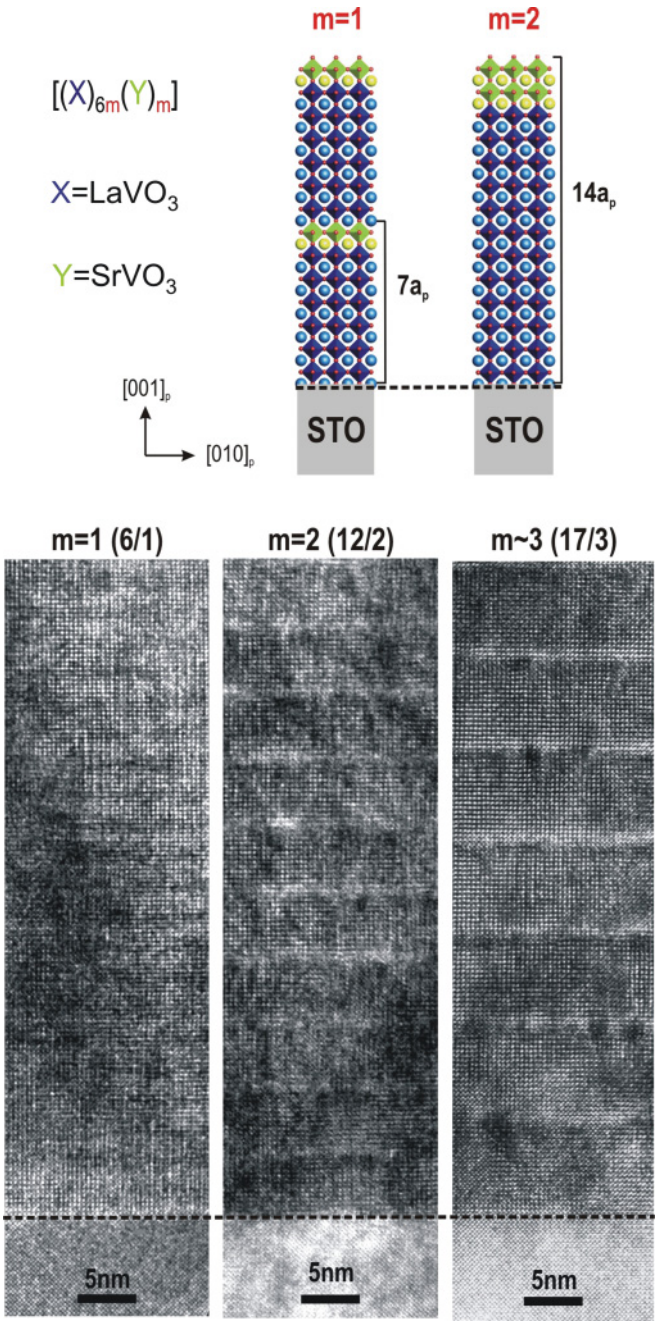


FIG. 1. (Color online) Top: Schematic showing the first two terms of an $[(X)_{6m}(Y)_m]$ series of superlattice. The composition is identical in both cases but the periodicity of the superlattice is different. Bottom: HREM images (JEOL 2010F) for the first three terms of the superlattices $(LaVO_3)_{6m}(SrVO_3)_m$, i.e., samples $m = 1$, $m = 2$, and close to $m = 3$, with a compound 17/3 (denoted $m \sim 3$).

## III. RESULTS AND DISCUSSION

Figure 1 shows three HREM images, recorded on the terms $m = 1$, 2, and 3 along the $[100]_p$ orientation of the substrate. The image of the superlattice for $m \sim 3$, shows a series of stacked layers, with thick and thin parts regularly alternating. Although it is tempting to associate the observed difference in contrast to $LaVO_3$ for the thicker part and to $SrVO_3$ for the lighter regions, the origin of contrast in HRTEM is not straightforward and depends on the imaging conditions. In the high-resolution HAADF STEM image obtained on an $m = 3$ sample and presented in Fig. 2, it is possible to confirm the realization of a $LaVO_3/SrVO_3$ superlattice because of the presence of strontium in the thinner $SrVO_3$ layer and lanthanum in the thicker $LaVO_3$ layer. For this $m = 3$ sample, the interface between the blocks of $LaVO_3$ and $SrVO_3$ shows steps of roughly 1 perovskite unit, preserving the continuity of the $SrVO_3$ layer. In comparison, if one looks at the images obtained on $m < 3$ samples (Fig. 1), it becomes difficult to assert the formation of a $LaVO_3/SrVO_3$ superlattice with flat interfaces, notably for the case where $m = 1$.

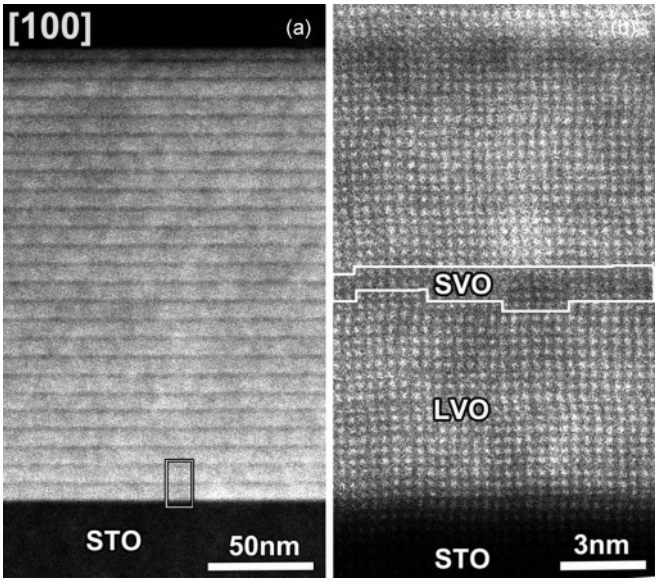


FIG. 2. (Color online) (a) Low-magnification HAADF-STEM image of an $m = 3$ (18/3) superlattice. (b) High-resolution HAADF-STEM image at the film/substrate interface. The $SrVO_3$ (SVO) layer is marked by its darker contrast compared to the surrounding $LaVO_3$ (LVO) layers. Note that there is some amount of roughness or atomic steps at the LVO/SVO interfaces.

SAED patterns obtained on this $m = 1$ sample [Fig. 3(a)] can actually provide more averaged information on the existence of a superlattice than the images presented in Fig. 1. First, the material under investigation ($SrTiO_3$ substrate and $LaVO_3/SrVO_3$ film) being structurally related to perovskite, the most intense reflections observed in these diffraction patterns are naturally associated with the perovskite subcell. Using the $[010]_p^*$ direction as the reference ($a_{STO} = 3.9$ Å), the parameter of the perovskite subcell along the $[001]_p^*$ direction perpendicular to the substrate is about 3.95 Å, in agreement with the results obtained by x-ray diffraction.[17] Along this same $[001]_p^*$ direction, one can observe reflections of a low intensity and organized on a regular basis on both sides of each of the reflections related to the perovskite subcell [see enlarged area in Fig. 3(b)]. These reflections can be considered satellite reflections and indexed using a vector of the form $q = (1/\Lambda)c^*$. They are associated with the periodic structure generated by the regular stacking of $LaVO_3$ and $SrVO_3$ in the superlattice. This allows us to calculate a superperiod $\Lambda$ corresponding to 27.1 Å that actually corresponds to 7 perovskite units as expected for this $m = 1$ term. In the

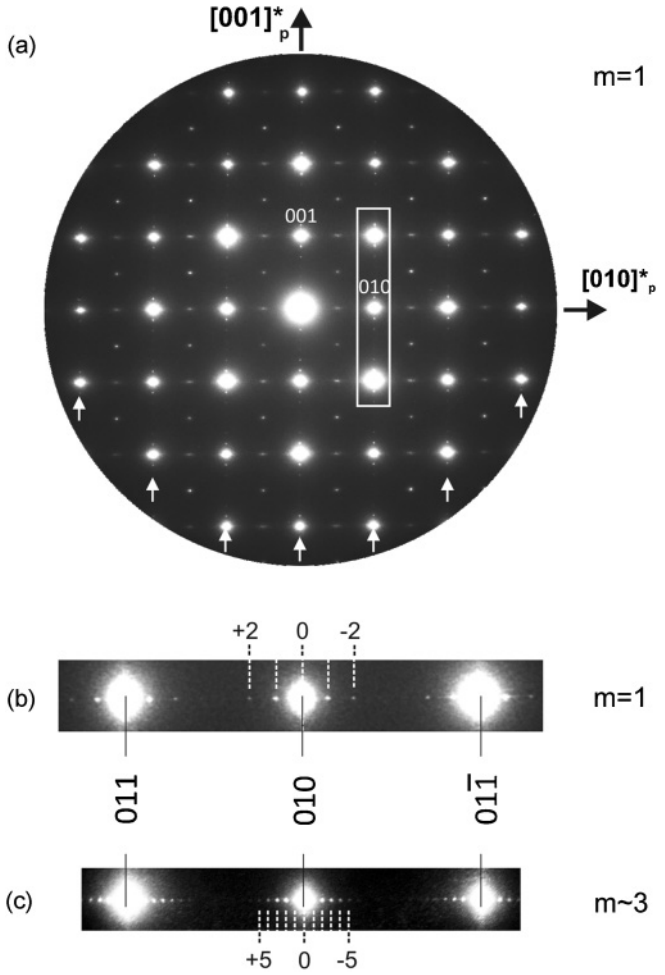


FIG. 3. (Color online) (a) $[100]_p$ SAED patterns from an $m = 1$ superlattice. The most intense reflections can be indexed in the perovskite subcell. Along $[001]_p$* (white arrows), satellite reflections appear systematically associated with reflections of the perovksite subcell. (b) Enlargement of the area within the white rectangle in (a). The measured periodicity is 27.1Å $\approx 7a_p$ and is therefore compatible with an $m = 1$ $(LaVO_3)_6/(SrVO_3)_1$ superlattice. (c) Enlargement of part of the $[100]_p$ SAED patterns from the $m \sim 3$ $(LaVO_3)_{17}/(SrVO_3)_3$ superlattice with a periodicity of 77.3Å $\approx 20a_p$.

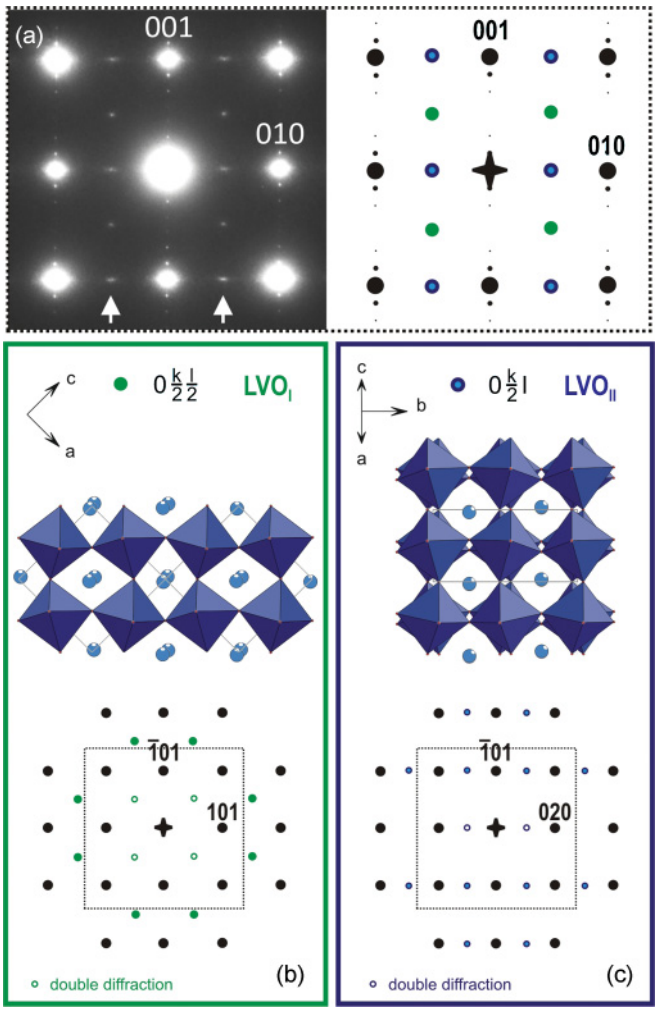


FIG. 4. (Color online) (a) Central area of a $[100]_p$ SAED pattern from an $m = 1$ superlattice and its schematic representation. The rows of additional reflections indicated by white arrows can be decomposed into two parts: (b) the first, located at the $0\frac{k}{2}\frac{l}{2}$ positions of the perovskite subcell, are compatible with a [010] zone axis pattern for $LaVO_3$ (orthorhombic Pnma bulk reference); (c) the second, located at the $0\frac{k}{2}l$ positions of the perovskite subcell, are consistent with a [101] zone axis pattern.

second example [Fig. 3(c)], several orders of sharp satellite spots are observed, indicative of the high-quality periodic structure of the deposited superlattices.

The diffraction pattern also provides information on the $LaVO_3$ component of the superlattice. Considering the reflections of the perovskite subcell and its satellites [Fig. 4(a)], there are indeed extra reflections whose presence cannot be explained on the basis of this description. The extra rows of reflections, marked by the two arrows in Fig. 4(a), can be separated into two subsets, located at positions $0\frac{k}{2}l$ and $0\frac{k}{2}\frac{l}{2}$. These reflections denote the presence of a superstructure as referred to a simple perovskite lattice. It can be explained if one considers that the $LaVO_3$ component of the superlattice presents a distorted perovskite structure involving rotation of the $VO_6$ octahedra consistent with those existing in bulk $LaVO_3$.[21] In this case, considering the existence of 90°-oriented domains, the reflections $0\frac{k}{2}\frac{l}{2}$ [Fig. 4(b)] and $0\frac{k}{2}l$ [Fig. 4(c)] may be associated, respectively, with [010] and [101] zone axes of a Pnma structure having cell parameters $a_p\sqrt{2} \times 2a_p \times a_p\sqrt{2}$. In Fig. 4, which schematically summarizes the analysis, we see that these two orientations correspond to the case where the $b$ axis of the Pnma $LaVO_3$ structure is parallel to the substrate plane but differs by an in-plane rotation of 90°. Considering its Pnma bulk form, the epitaxial relationship for LVO can be written as (101)LVO ∥ (001)STO/SVO, with [010]LVO ∥ [100]STO/SVO for $LVO_I$ and [010]LVO ∥ [010]STO/SVO for $LVO_{II}$.[22] Notably we do not observe the orientation variant (010)LVO ∥ (001)STO/SVO with [101] ∥ [010]STO/SVO that would have the $b$-axis perpendicular to the plane of the substrate [see an illustration in our recent study of Pnma $BiCrO_3$ films deposited on (100)-$SrTiO_3$].[23] For the various samples observed by TEM and corresponding to the values $m = 1$, 2, 3, and 7, SAED patterns confirm the

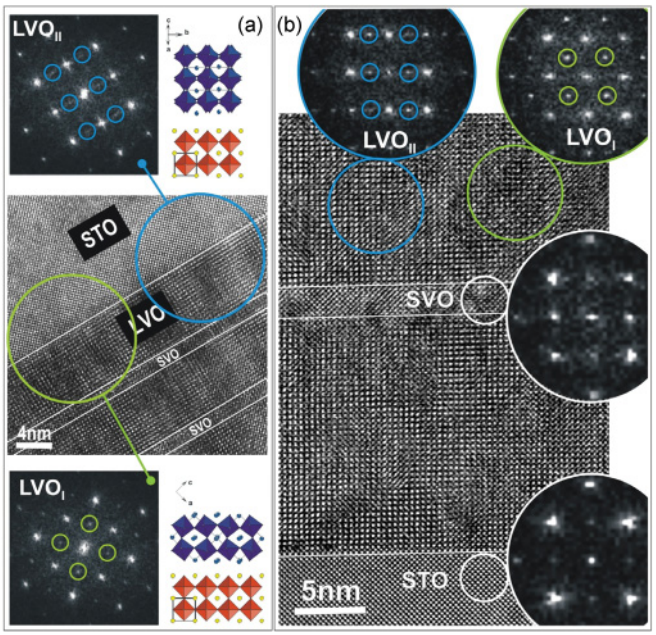


FIG. 5. (Color online) HREM images of the film/substrate interface for two samples in the series $(LaVO_3)_{6m}(SrVO_3)_m$, with (a) $m \sim 3$ and (b) $m = 7$. For each sample, Fourier transforms performed on the circled areas show that $LaVO_3$ layers are formed by the imbrication of $LVO_I$- and $LVO_{II}$-oriented domains.

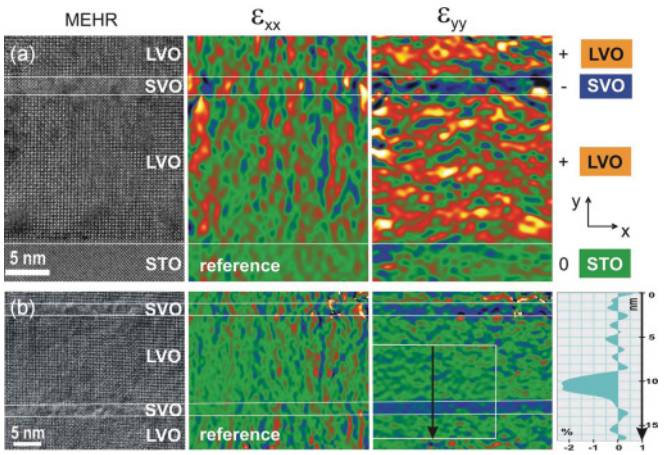


FIG. 6. (Color online) (a) HREM image of the film/substrate interface for a 135-nm-thick $m = 7$ superlattice and the local deformations obtained by the GPA method along the in-plane ($\varepsilon_{xx}$) and out-of-plane ($\varepsilon_{yy}$) directions. Reference is made to the STO substrate. Compared to the substrate chosen as the reference area, green coloring indicates no change; blue, a negative deformation; and red-orange, a positive deformation. (b) HRTEM image of LVO/SVO interfaces (middle of the film) and the associated local deformations $\varepsilon_{xx}$ and $\varepsilon_{yy}$. Reference is made here to the LVO layer. The profile across the ~3-nm-thick SVO layer indicates a deformation of about −2.2%.

existence of a perovskite distorted structure with orientation domains for the $LaVO_3$ layer even for $m = 1$, where the $LaVO_3$ layers are about 6 u.c. thick. While such structural features have not been reported, to our knowledge, in ultrathin $LaVO_3$ films, we find similarity to recent works on ultrathin $LaMnO_3$ films[24] and on $LaMnO_3/SrMnO_3$[25] superlattices, where 10- to 12-u.c. $LaMnO_3$ layers are shown to adopt a distorted perovskite structure with octahedral tilting comparable to what is observed in bulk $LaMnO_3$ (and so $LaVO_3$). In Figs. 5(a) and 5(b), corresponding to $m \sim 3$ and $m = 7$ samples, respectively, HREM images and associated Fourier transforms reveal that the two $LVO_I$ and $LVO_{II}$ orientations are present concurrently in every $LaVO_3$ layer, including the first deposited. The 90°-oriented domains appear on a local scale as indicated by the Fourier transform characteristics of the two $LVO_I$ and $LVO_{II}$ variants. In Fig. 5(b), the contrast in the $SrVO_3$ layer appears to be uniform and the Fourier transform is similar to that of the $SrTiO_3$ substrate.

While it is clear that our superlattices are epitaxially grown on (100)-$SrTiO_3$, the question whether the films are fully strained by the substrate actually remains. Figure 6 represents the result of the GPA performed on an $m = 7$ $(LaVO_3)_{6m}(SrVO_3)_m$ superlattice. In Fig. 6(a), for the deformations along the direction parallel to the substrate ($\varepsilon_{xx}$), we see that there is no difference in contrast between the substrate chosen as reference and the first two LVO/SVO layers. This indicates that both compounds are strained in-plane and they have adopted the parameters of $SrTiO_3$. In Fig. 6(b), showing LVO/SVO interfaces, the same phenomenon is observed, reflecting the fact that the in-plane strain is kept throughout the film thickness. If we now look at the images that correspond to out-of-plane deformations ($\varepsilon_{yy}$), we notice a difference. The $LaVO_3$ part is affected by a dilatation in the direction perpendicular to the substrate, while $SrVO_3$ is under a compressive strain taking $SrTiO_3$ as a reference. If one refers to the parameters of the bulk $LaVO_3$ ($\langle a_p \rangle = 3.925$ Å) and $SrVO_3$ ($a = 3.843$ Å), the relative difference from $SrTiO_3$ ($a = 3.905$ Å) is of −0.5% and 1.6%, respectively. We can therefore assume that $LaVO_3$ has a slight compression in the plane, which results in an out-of-plane expansion of its lattice spacing, in contrast to the $SrVO_3$ layers, where epitaxy requires an in-plane expansion of the lattice, which induces an out-of-plane compression. GPA is a quantitative method that allows us to obtain an estimate of the relative deformation experienced by the $SrVO_3$ layer taking the $LaVO_3$ layer as the reference [Fig. 6(b)]. The measure indicates that the out-of-plane lattice parameter of the $SrVO_3$ layer is about 2.2% smaller than that of the surrounding $LaVO_3$ layers. It should be noted, however, that here we are within the limit of this type of analysis in the sense that the deformations are relatively small. This explains the noisy appearance of the deformation images obtained in Fig. 6. The analysis of smaller terms ($m < 3$) has proven to be even more difficult. Nevertheless, we can estimate that such an achievement for an $m = 7$ term is quite representative of our films.

Finally, EELS spectra were recorded on an $m = 3$ sample with an STEM probe scanning across the layers. This means that all spectra are collected under the same experimental conditions. Because the $SrVO_3$ layer is very thin and the spatial resolution of the probe is limited (≈1 nm), the spectrum for the $SrVO_3$ layer shows some residual La signal but the amount is considerably smaller than for the $LaVO_3$ layer [Fig. 7(a)]. This effect will also cause the differences in the spectra of the two types of layers to be less pronounced. However, the superposition of the $LaVO_3$ signal onto the $SrVO_3$ spectrum can be partially eliminated by subtracting

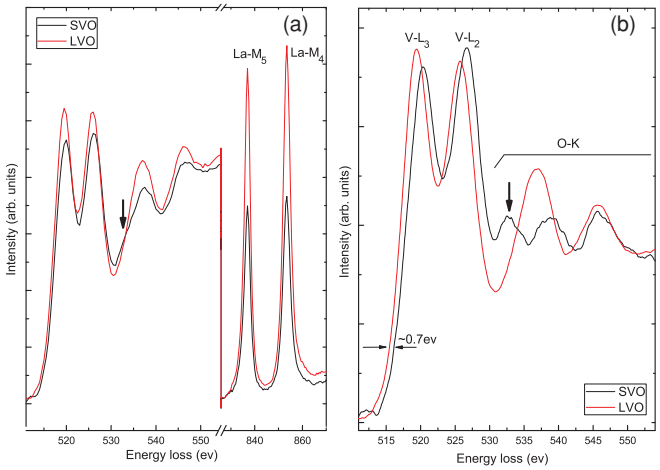


FIG. 7. (Color online) Probe scanning EELS spectra in STEM mode for $SrVO_3$ and $LaVO_3$ layers from an $m = 3\,(18/3)$ superlattice. (a) $SrVO_3$ and $LaVO_3$ spectra with the background removed before the V $L_{23}$ edge and the energy aligned by cross-correlation to the La $M_5$ peak (present in the $SrVO_3$ layer as well because of the spatial resolution limitations and signal delocalization). (b) $SrVO_3$ and $LaVO_3$ spectra (V $L_{23}$ edge and O $K$ edge) after plural scattering removal. The $SrVO_3$ spectrum is subtracted from the weighted $LaVO_3$ spectrum to eliminate the effect of overlap.

a weighted $LaVO_3$ spectrum until the La signal is completely removed. Figure 7(b) shows the $SrVO_3$ spectrum after such treatment, together with the $LaVO_3$ spectrum (power-law background and plural scattering are removed in advance). The V $L_{23}$ edge of $SrVO_3$ is clearly shifted approximately 0.7 eV to higher energies with respect to that of $LaVO_3$. The height ratio of the $L_2/L_3$ peak of V is also higher in the $SrVO_3$ spectrum than in the $LaVO_3$ spectrum. Both the chemical shift and the $L_{2,3}$ ratio change demonstrate a higher V valence in the $SrVO_3$ layer compared to that of the $LaVO_3$ layers.[26,27] Furthermore, compared to the $LaVO_3$ spectrum [Fig. 7(a)], the valley between the V $L_2$ peak and the O $K$ edge is shallower for $SrVO_3$ and the first peak of the O $K$ edge is broader. An extra prepeak on the O $K$ edge is clearly separated after removal of the $LaVO_3$ signal [marked by a black arrow in Fig. 7(b)]. The two fine structures derived mainly agree with Ref. 28. On the one hand, the first peak of the O $K$ edge of $SrVO_3$ [Fig. 7(b), indicated by an arrow] shows a further split in Ref. 28 that is slightly recognizable in our spectrum as well. On the other hand, the width of the $SrVO_3$ V $L_{23}$ edge is much broader than that of $LaVO_3$ in Ref. 28, but they are almost the same in our spectra. Both differences, especially the latter one, may be related to a change in electronic structure at the interface but this is difficult to interpret directly from the spectrum and requires further density functional calculations.

## IV. CONCLUSION

TEM investigations confirm the general structural quality of the samples and the formation of strained $(LaVO_3)_{6m}(SrVO_3)_m$ superlattices. The layers are homogeneously flat and chemically well defined. The superlattices are found to be epitaxially grown and show satellite reflections in the diffraction pattern in good agreement with the periodicities targeted by varying the $m$ value. At the atomic level, however, there are atomic steps at the $LaVO_3/SrVO_3$ interfaces that could conduct to discontinuities in the $SrVO_3$ layers for the lower, $m = 2$ and $m = 1$ terms. This amount of roughness is, however, in agreement with the picture of $SrVO_3$ acting as geometrically confined dopant layers.[18] For all the investigated superlattices ($m$ = 1–7), the $LaVO_3$ layers are made of coherently grown 90°-oriented domains whose structures present tiltings of the octahedra compatible with what is observed in bulk $LaVO_3$. This assumption is mostly motivated by the similarity of the observed SAED patterns and HREM images to those expected for bulk $LaVO_3$. Based on GPA results obtained on an $m = 7$ superlattice, the $SrVO_3$ layers appear to be in compressive strain, leading to a tetragonal distortion with a shrinking of the out-of-plane parameter compared to the bulk. EELS investigations indicate changes in the fine structure of the V $L_{23}$ edge, related to a valence change between the $LaVO_3$ and the $SrVO_3$ layers. The exact amount of this change is unknown at present and would require further studies. The existence of a mixed valence in adjacent $VO_2$ sheets with partially localized electrons cannot be inferred from the present work. The resolution of the current STEM-EELS experiment is somewhat limited and does not allow us to look at the $V$-edge changes within the different unit cells of the $SrVO_3$ layer. Moreover, the limited flatness of the interfaces would create a smeared-out EELS signature even with a smaller probe size.

## ACKNOWLEDGMENTS

This work was carried out in the frame of the STREP MACOMUFI (Grant No. NMP4-CT-2006-313321) supported by the European Commission and by the CNRS, France. Financial support from the C'Nano Nord-Ouest (2975) and PHC STAR (21465YL) projects is also acknowledged. P.B. acknowledges financial support from the French CNRS and CEA METSA network for the realization of GPA analyses at CEMES. H.T. would like to acknowledge the financial support from FWO-Vlaanderen (Project No. G.0147.06). J.V. also acknowledges financial support from the European Union under the Framework 6 program through a contract for an Integrated Infrastructure Initiative (Reference 026019 ESTEEM).

[1] A. Ohtomo and H. Y. Wang, Nature **427**, 423 (2004).
[2] S. Thiel, G. Hammerl, A. Schmehl, C. W. Schneider, and J. Mannhart, Science **313**, 1942 (2006).
[3] Y. Hotta, T. Susaki, and H. Y. Hwang, Phys. Rev. Lett. **99**, 236805 (2007).
[4] M. Basletic, J.-L. Maurice, C. Carrétéro, G. Herranz, O. Copie, M. Bibes, E. Jacquet, K. Bouzehouane, S. Fusil, and A. Barthélémy, Nat. Mater. **7**, 621 (2008).
[5] M. Huijben, G. Rijnders, D. H. A. Blank, S. Bals, S. Van Aert, J. Verbeeck, G. Van Tendeloo, A. Brinkman, and H. Hilgenkamp, Nat. Mater. **5**, 556 (2006).

[6]A. Brinkmann, M. Huijben, M. van Zalk, J. Huijben, U. Zeitler, J. C. Maan, W. G. van der Wiel, G. Rijnders, D. H. A. Blank, and H. Hilgenkamp, Nature **6**, 493 (2007).
[7]N. Reyren, S. Thiel, A. D. Caviglia, L. Fitting Kourkoutis, G. Hammerl, C. Richter, C. W. Schneider, T. Kopp, A.-S. Rüetschi, D. Jaccard, M. Gabay, D. A. Muller, J.-M. Triscone, and J. Mannhart, Science **317**, 1196 (2007).
[8]C. N. R. Rao and B. Raveau, *Colossal Magnetoresistance, Charge Ordering and Related Properties of Manganese Oxides* (World Scientific, Singapore, 1998).
[9]M. Imada, A. Fujimori, and Y. Tokura, Rev. Mod. Phys. **70**, 1039 (1998).
[10]J. H. Park, E. Vescovo, H.-J. Kim, C. Kwon, R. Ramesh, and T. Venkatesan, Nature **392**, 794 (1998).
[11]S. Miyasaka, Y. Okimoto, M. Iwama, and Y. Tokura, Phys. Rev. B **68**, 100406 (2003).
[12]V. Giannakopoulo, P. Odier, J. M. Bassat, and J. P. Loup, Solid State Commun. **93**, 579 (1995).
[13]M. Sayer, R. Chen, R. Fletcher, and A. Mansingh, J. Phys. C Solid State Phys. **8**, 2059 (1975).
[14]F. Inaba, T. Arima, T. Ishikawa, T. Katsufuji, and Y. Tokura, Phys. Rev. B **52**, R2221 (1995).
[15]S. Miyasaka, T. Okuda, and Y. Tokura, Phys. Rev. Lett. **85**, 5388 (2000).
[16]W. C. Sheets, B. Mercey, and W. Prellier, Appl. Phys. Lett. **91**, 192102 (2007).
[17]W. C. Sheets, P. Boullay, U. Lüders, B. Mercey, and W. Prellier, Thin Solid Films **517**, 5130 (2009).
[18]U. Lüders, W. C. Sheets, A. David, W. Prellier, and R. Frésard, Phys. Rev. B **80**, 241102 (2009).
[19]M. J. Hÿtch, Microsc. Microanal. Microstruct. **8**, 41 (1997).
[20]M. J. Hÿtch, E. Snoeck, and R. Kilaas, Ultramicroscopy **74**, 131 (1998).
[21]P. Bordet, C. Chaillout, M. Marezio, Q. Huang, A. Santoro, S. W. Cheong, H. Takagi, C. S. Oglesby, and B. Batlogg, J. Solid State Chem. **106**, 253 (1993).
[22]Notice that a strict strained growth of either $LVO_I$ or $LVO_{II}$ on large domains on $SrTiO_3$ would imply a distortion of the orthorhombic cell since the 90° angle between the [100] and the [001] directions cannot be maintained considering these epitaxial relations.
[23]A. David, P. Boullay, R. V. K. Mangalan, N. Barrier, and W. Prellier, Appl. Phys. Lett. **96**, 221904 (2010).
[24]C. Aruta, G. Ghiringhelli, V. Bisogni, L. Braicovich, N. B. Brookes, A. Tebano, and G. Balestrino, Phys. Rev. B **80**, 014431 (2009).
[25]A. B. Shah, Q. M. Ramasse, S. J. May, J. Kavich, J. G. Wen, X. Zhai, J. N. Eckstein, J. Freeland, A. Bhattacharya, and J. M. Zuo, Phys. Rev. B **82**, 115112 (2010).
[26]M. Varela, M. P. Oxley, W. Luo, J. Tao, M. Watanabe, A. R. Lupini, S. T. Pantelides, and S. J. Pennycook, Phys. Rev. B **79**, 085117 (2009).
[27]H. D'Hondt, J. Hadermann, A. M. Abakumov, A. S. Kalyuzhnaya, M. G. Rozova, A. A. Tsirlin, R. Nath, H. Tan, J. Verbeeck, E. V. Antipov, and G. Van Tendeloo, J. Solid State Chem. **182**, 356 (2009).
[28]L. F. Kourkoutis, Y. Hotta, T. Susaki, H. Y. Hwang, and D. A. Muller, Phys. Rev. Lett. **97**, 256803 (2006).